EUROPHYSICS LETTERS 15 June 2004

Europhys. Lett., **66** (6), pp. 785–791 (2004)
DOI: 10.1209/epl/i2003-10268-x

Frustrated energy transport through micro-waveguides decorated by gold nanoparticle chains

R. Quidant[1,2], G. Lévêque[3], J.-C. Weeber[2], A. Dereux[2], C. Girard[4] and J. Weiner[3]

[1] *ICFO, Institut de Ciències Fotòniques - Jordi Girona 29, Nexus II 08034 Barcelona, Spain*
[2] *LPUB, UMR-CNRS 5027 - 9 avenue A. Savary, F-21078 Dijon, France*
[3] *LCAR, UMR-CNRS 5589, Université Paul Sabatier - 31062 Toulouse, France*
[4] *CEMES, UPR-CNRS 8011 - 29 Rue Jeanne Marvig, BP4347 F-31055 Toulouse, France*

(received 5 December 2003; accepted in final form 20 April 2004)

PACS. 07.79.Fc – Near-field scanning optical microscopes.
PACS. 73.20.Mf – Collective excitations (including excitons, polarons, plasmons and other charge-density excitations).
PACS. 78.66.Bz – Metals and metallic alloys.

Abstract. – This letter reports near-field optical observations of light energy transport along micro-waveguides decorated by short chains of gold "nanodots". In spite of their subwavelength dimensions (100 nm diameter ×20 nm height), the metallic dots in the chain function as an efficient photonic band filter or a *nanometric Bragg mirror*. Numerical simulations reproduce the observed phenomenon and indicate that the occurrence of a band gap for light transport through the decorated guide corresponds to a selective absorption by the metallic chain.

The ability to control and mold light flux at a subwavelength scale would have significant practical consequences for the prospects of integrated optical-device miniaturization. During the last decade, among the different routes explored to achieve this integration, surface plasmon polaritons (SPPs) supported by noble-metal nanostructures have offered several promising opportunities [1]. These polariton modes involve collective excitations of the free-electron gas confined inside metals, and they depend critically on the design of the metallic nano-objects supporting the polariton propagation. In recent years, two well-identified classes of experimental studies have been reported. i) The first class of applications is based on continuous structures in one or two dimensions (metallic films, stripes, or wires). In these systems the SPPs, that correspond to the propagation of electron density oscillations, can be directly used for optical-signal transfer. Plasmon propagation along metallic stripes with micrometer width has been investigated both theoretically [2,3] and experimentally [4–6]. More recently, in agreement with previous calculations [7], Krenn *et al.* have reported experimental evidence for the propagation of near-infrared light along nanowires featuring subwavelength cross-sections [8]. ii) The second class of structures implements periodic arrays of metallic

nanoparticles (chains, 2D arrays, ...) [9–11]. In fact, each individual nanostructure confines the electron gas in three dimensions and gives rise to "localized surface plasmons" (LSPs). These periodic structures exhibit resonances associated with a significant increase of both absorption and scattering phenomena. In the quasi-static limit, *i.e.* for particle size much smaller than the incident wavelength, the plasmon oscillations correspond to the first multipolar excitations. When such nanoparticles are assembled to form a finite chain, depending on the interparticle distances, two kinds of interaction can be identified. For closely packed particle arrays, the coupling arises from the evanescent fields tailing off each individual particle (evanescent coupling). Calculations performed by Quinten *et al.* [12] have shown that this type of coupling could be optimized to promote the transport of visible light through linear chains of silver nanoparticles with diameters typically scaled down to 30 nm. Very recently, direct experimental evidence of this short-range coupling has been reported [13] by measuring electromagnetic energy transport along silver nanoparticle plasmon waveguides.

For objects separated by distances greater than a few tenths of nanometers, the interaction relies on the interference of their scattered dipolar fields (dipole-dipole or far-field coupling). In this long-range regime, a large 2D periodic array of particles decorating a metallic film enables the creation a photonic band gap for the surface plasmon polariton mode supported by the structure [14]. This effect has been used to propagate light waves along straight and bent lines of defects [15].

In a related technique, efficient light signal transport can also be achieved with high optical index dielectric micro-waveguides (MWGs) featuring submicron transverse cross-sections. Nevertheless, when the lateral dimensions of the MWG enter the subwavelength domain, recent experimental work shows that one should use optical evanescent fields, coupling to one of the waveguide extremities, rather than conventional propagating laser beams. Such evanescent sources can be easily produced by focusing a Gaussian beam incident on the transparent substrate in such a way that it is totally reflected when there is no structure deposited on the surface of the substrate [16].

In this paper, we combine these two technologies (MWGs plus plasmon-polariton metallic chains). In particular, we show that short linear arrays of gold dots microfabricated on the top surface of such MWGs dramatically modify the light transmission spectrum through the structure and select bands of wavelengths as it would be made with a *nanometric Bragg mirror* operating at visible wavelengths. The microfabrication of our prototype comprises two steps of e-beam lithography combined with a dry etching process. We start from a 150 nm thick TiO_2 (index of refraction $n = 2.41$) layer deposited by assisted ion beam deposition onto a BK7 glass substrate. First, the e-beam patterning of the host TiO_2 MWG was performed by a SEM microscope JEOL 840-A operating at 20 keV on a layer of polymethylmethacrylate (PMMA) resist (950×10^3 molecular weight and 150 nm thickness). After removing of the PMMA film zones that have been irradiated by the electronic beam, a 40 nm nickel coating is evaporated onto the surface sample. The remaining PMMA regions are then lifted off by dissolution, and reactive ion etching of the TiO_2 layer is performed in a GIR 300 ALCATEL system. The etching process uses a $SF_6(5/6)/Ar(1/6)$ equal-flow-rate gas mixture at a pressure of 0.015 mbar and rf power of 40 W. Then, the remaining Ni mask is removed in nitric acid solution. The patterning of the gold nanodots requires a second e-beam lithography operation. At this stage, the main difficulty is a precise positioning of the sample required for the dots to be aligned along the MWG. A satisfactory alignment can be easily attained for MWGs with widths ≥ 600 nm. A scanning electron microscope image of the device is presented in fig. 1.

The optical characterization of the micro-fabricated structure has been performed with a Photon Scanning Tunnelling microscope (PSTM) [17–19]. An optical fiber is piezoelectrically driven so as to act as local probe of the optical field in the near-field zone [20]. Conversely,

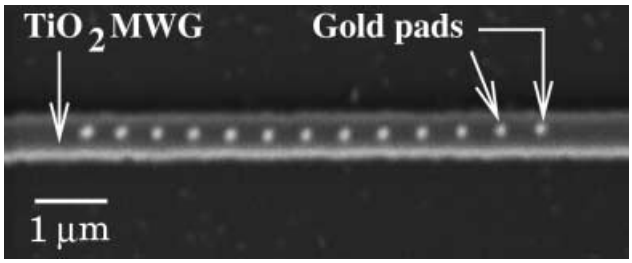

Fig. 1 – Scanning electron microscope image of the micro-fabricated structured MWG. The TiO_2 linear guide is 600 ± 20 nm wide, 150 ± 5 nm high and $50\,\mu$m long. The metallic chain consists of 13 gold nanostructures (diameter 100 ± 20 nm, height = 20 nm) periodically arranged with an interval a of 600 ± 20 nm.

such probes can also be used for the remote optical addressing of single nano-objects [21]. The probes we used have been coated with 7 nm of Cr in order to reduce the contribution of scattered radiative fields in the detection process. In our experiments the PSTM probe was scanned at constant height. In this configuration, the signal detected is well known to be related to the spatial distribution of the intensity of the local electric field. The waveguide is locally excited, as in fig. 2, by a focused laser beam totally reflected at the substrate interface. This local illumination is produced by injecting a laser beam into a focusing single-mode optical fiber (NA = 0.17), working at the focal distance = 18 mm. When shining a Gaussian beam in the total internal reflection setup used here, one may expect to exploit the Goos-Hänschen shift which results in the fact that the incident and reflected beams are not symmetrical with respect to the focal point. In the air side of the air-glass interface, a wave vector parallel to the surface of the substrate is associated with this effect. The Gaussian beam is focused at the right extremity of the MWG in such a way that the components of the incident wave vector parallel to the surface of the substrate be aligned along the longitudinal axis of the MWG (fig. 2). Let us note that this condition is much easier to meet than the alignment of all three components of the incident wave vector. To optimize the light transfer, the incident light field is p-polarized (also called Transverse Magnetic polarization) and the reflection angle is fixed at 50°. The evanescent light spot lying at the glass-air interface features an elliptic shape

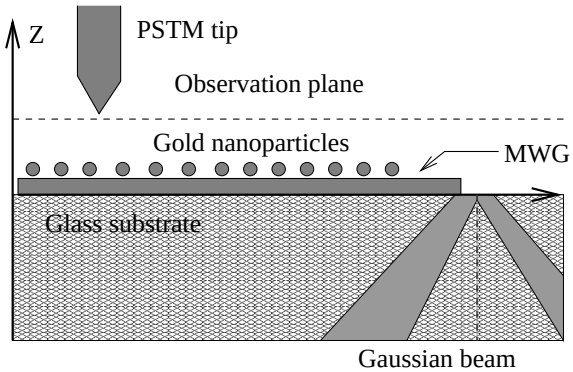

Fig. 2 – A MWG lying on the surface of a substrate is illuminated by a Gaussian beam reflected at the interface between the substrate and the outside medium.

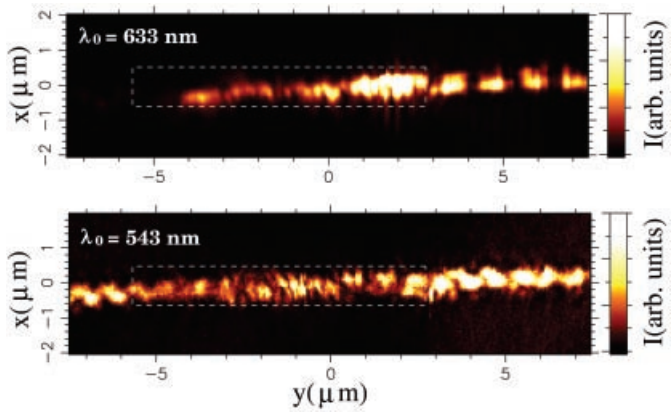

Fig. 3 – PSTM images recorded at 50 nm above the structure of fig. 2 for two different wavelengths, $\lambda_0 = 633\,\text{nm}$ and $\lambda_0 = 543\,\text{nm}$. The dashed-line frame outlines the area occupied by the metal particles.

with a long axis of $12\,\mu$m along the incident direction and a short axis of $8\,\mu$m [22]. In this configuration, the light flux launched inside the MWG propagates also along the upper side of the guide and couples with the region decorated by the gold nanoparticles. Maps in fig. 3 show two typical PSTM measurements recorded for two different incident wavelengths $\lambda_0 = 633\,\text{nm}$ and $\lambda_0 = 543\,\text{nm}$ above the sample described in fig. 1. In both images, the dashed-line frame indicates the area of the TiO_2 MWG which is decorated by the gold nanodots. For each wavelength, the distribution of the electric near-field intensity before the structured zone ($y > 2.8\,\mu$m) exhibits large periodic patterns, with periods of about 650 nm for $\lambda_0 = 543\,\text{nm}$ and about $1\,\mu$m for $\lambda_0 = 633\,\text{nm}$. These beatings indicate the interference of several excited transverse and longitudinal modes that propagate within the structure.

At the wavelength $\lambda_0 = 543\,\text{nm}$, the light energy flow is not significantly altered by the presence of the gold chain on the top face of the host MWG. Around this energy range, the

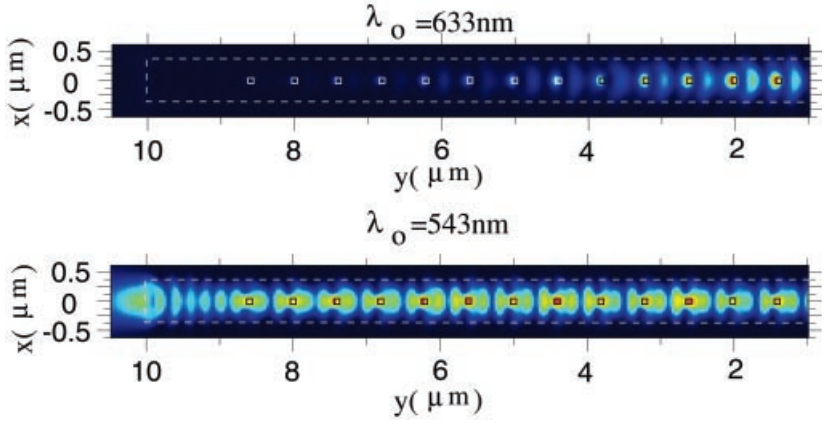

Fig. 4 – Electric near-field intensity maps calculated over the device for two different incident wavelengths (top $\lambda_0 = 633\,\text{nm}$, bottom $\lambda_0 = 543\,\text{nm}$). The dashed-line frame localizes the metallic chain.

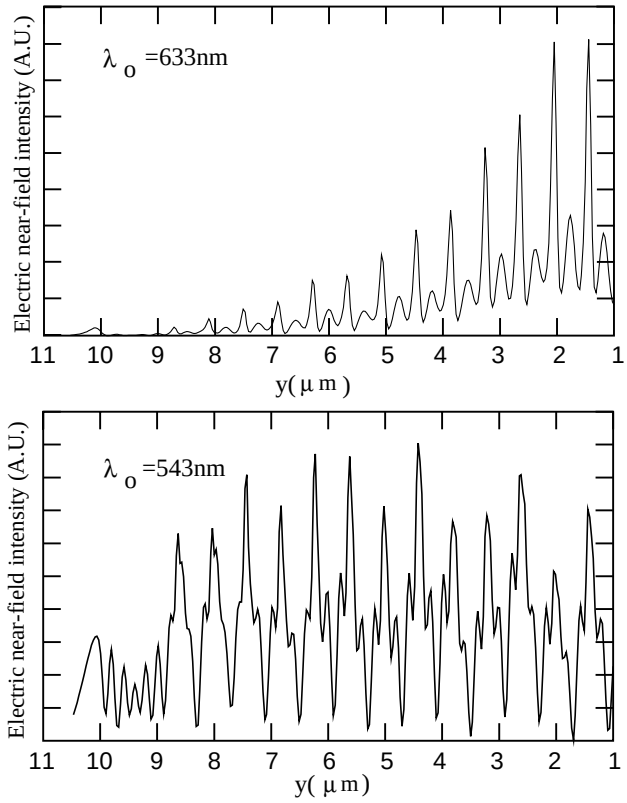

Fig. 5 – Two lateral cross-sections corresponding to the two maps of fig. 4.

device exhibits a high level of light transmission with only small energy leakage (estimated at less than 10%). In contrast, when working around $\lambda_0 = 633\,\text{nm}$, the light transport inside the MWG is frustrated. In this *stopping regime* the high spatial resolution of the PSTM permits two features to be clearly distinguished:

i) The energy guided by the MWG progressively vanishes after a propagation length of about $7\,\mu$m along the metal chain.

ii) In contrast to the behavior of a *conventional* Bragg mirror, no significant increase of the interference pattern occurs before entering the zone occupied by the periodic line of metal dots.

Therefore, we do not believe that the appearance of a stop-band around $\lambda_0 = 633\,\text{nm}$ is the result of conventional interference phenomena, but rather is produced by the presence, in this wavelength range, of highly absorbing plasmon modes coupled to the MWG. We conclude that the frustrated light transmission associated with the decorated MWG is due to strong coupling of the field propagating in the TiO_2 core with surface plasmon modes of the gold chain that induce important radiative and non-radiative signal losses near the resonant frequency of the metallic chain. The increase of the PSTM intensity observed at the beginning of the decorated region (cf. fig. 3 with $\lambda_0 = 633\,\text{nm}$) reveals these radiative signal losses. At this point, it is worthwhile to complete our analysis with numerical simulations. The physical mechanisms that govern the intensity of the energy flow are complex and must be described with a realistic description of the decorated MWG. To solve the difficulties related to the pres-

ence of both nanometric (for describing the gold dots) and micrometric scales (for the MWG) we have applied the *localized dyadic Green function method* [16]. Such *ab initio* calculations of the optical near-field distributions only require a specification of the frequency-dependent dielectric constant and the precise shape of the lithographically designed structures [23]. Consequently, they can stand alone, complement and even anticipate experimental studies. Under some circumstances, it is possible with this method to perform computational experiments before effective realization in the laboratory. In this letter, we have simulated the observed penetration of light inside the TiO_2 MWG decorated with a chain of 13 gold dots. We have considered the geometry depicted in fig. 2. First, we start from the known solutions $\boldsymbol{E}_0$ associated with a simple planar optical junction excited beyond the critical angle for total reflection by a focused laser beam. The spatial distribution of this *evanescent light spot* can be described from previous modelings [24]. The numerical procedure considers any object deposited on the surface as a localized perturbation which is discretized in direct space over a predefined volume mesh of N points $\{\boldsymbol{R}_i\}$. In a first step, the electric-field distribution $\boldsymbol{E}(\boldsymbol{R}_i, \omega)$ is determined self-consistently inside the perturbations (*i.e.*, the source field). At this stage, a standard renormalization procedure associated with the depolarization effect is applied to take care of the self-interaction of each discretization cell [25]. The final step relies on the Huygens-Fresnel principle to compute the electromagnetic field $\boldsymbol{E}(\boldsymbol{r}, \omega)$ on the basis of the knowledge of the self-consistent field inside the localized perturbations $\boldsymbol{E}(\boldsymbol{R}_i, \omega)$.

From this scheme, we present in figs. 4, 5 the near-field patterns computed for the two experimental wavelengths $\lambda_0 = 633\,\text{nm}$ and $\lambda_0 = 543\,\text{nm}$ at a constant height 50 nm above the top of the decorated MWG. According to experimental data, for $\lambda_0 = 633\,\text{nm}$ the intensity dramatically decreases along the first seven microns while the $\lambda_0 = 543\,\text{nm}$ regime exhibits efficient light transport along the whole length of the structure. Despite the strong scattering occurring around the gold dots, the optical near-field remains well confined inside the MWG. Finally, the absence for $\lambda_0 = 633\,\text{nm}$ of strong reflection at the input extremity of the gold nanodot chain (not represented in figs. 4, 5) confirms that the signal extinction does not result from a conventional Bragg mirror reflection.

To conclude, we have shown in this work that a periodic arrangement of nanometer-sized metal dots can selectively influence light energy transport inside the core of optical microwaveguides. In spite of its extremely reduced cross-section ($100\,\text{nm} \times 20\,\text{nm}$), the decorated MWG acts as an efficient photonic band filter functioning as a *nanometric Bragg mirror*. In the case of gold chains, the optical near-field measurements, performed with a PSTM, have revealed a *high* and *low* transmission regime. Numerical simulations based on the calculations of electric near-field intensity maps reproduce the complete phenomenon and indicate that the occurrence of a stop-band corresponds to a selective absorption by the periodic chain of metal dots. This new kind of structure, combining dielectric and metallic properties, should stimulate applications in integrated optics, especially for the realization of compact linear filters. Subsequent research will investigate the respective influence of various parameters (particle geometry, constitutive metal and waveguide dispersion) in order to tailor precisely the optical pass band of the device.

REFERENCES

[1] Barnes W. L., Dereux A. and Ebbesen T. W., *Nature*, **424** (2003) 824.
[2] Weeber J. C. *et al.*, *Phys. Rev. B*, **60** (1999) 9061.
[3] Berini P., *Phys. Rev. B*, **61** (2000) 10484.
[4] Charbonneau R., Berini P., Berolo E. and Lisicka-Shrzek E., *Opt. Lett.*, **25** (2000) 844.
[5] Lamprecht B. *et al.*, *Appl. Phys. Lett.*, **79** (2001) 51.

[6] Weeber J. C. *et al.*, *Phys. Rev. B*, **64** (2001) 045411.
[7] Takahara J. *et al.*, *Appl. Phys. Lett.*, **22** (1997) 475.
[8] Krenn J. R. *et al.*, *Europhys. Lett.*, **60** (2002) 663.
[9] Krenn J. R. *et al.*, *Phys. Rev. Lett.*, **82** (1999) 2590.
[10] Maier S. A., Brongersma M. L., Kik P. G. and Atwater H. A., *Phys. Rev. B*, **65** (2002) 193408.
[11] Brongersma M. L., Hartman J. W. and Atwater H. A., *Phys. Rev. B*, **62** (2000) R16356.
[12] Quinten M., Leitner A., Krenn J. R. and Aussenegg F. R., *Opt. Lett.*, **23** (1998) 1331.
[13] Maier S. A. *et al.*, *Nature Mater.*, **2** (2003) 229.
[14] Kitson S. C., Barnes W. L. and Sambles J. R., *Phys. Rev. Lett.*, **77** (1996) 2671.
[15] Bozhevolnyi S. I. *et al.*, *Phys. Rev. Lett.*, **86** (2001) 3009.
[16] Quidant R. *et al.*, *Phys. Rev. E*, **65** (2002) 036616.
[17] Reddick R. C., Warmack R. J. and Ferrell T. L., *Phys. Rev. B*, **39** (1989) 767.
[18] Reddick R. C. *et al.*, *Rev. Sci. Instrum.*, **61** (1990) 3669.
[19] Courjon D., Sarayedine K. and Spajer M., *Opt. Commun.*, **71** (1989) 23.
[20] Dereux A., Girard C. and Weeber J. C., *J. Chem. Phys.*, **112** (2000) 7775.
[21] Brun M., Drezet A., Mariette H., Chevalier N., Woehl J. C. and Huant S., *Europhys. Lett.*, **64** (2003) 634.
[22] Quidant R. *et al.*, *Europhys. Lett.*, **57** (2002) 191.
[23] Lévêque G. *et al.*, *Phys. Rev. E*, **65** (2002) 036701-8.
[24] Baida F., Labeke D. and Vigoureux J. M., *Ultramicroscopy*, **71** (1998) 351.
[25] Yaghjian A. D., *Proc. IEEE*, **68** (1980) 248.